

# Focused-Ion-Beam Induced Paramagnetic Defects in FAMn:PbI<sub>3</sub> Perovskite Films

Nam Joong Jeon<sup>1</sup>, Jangwon Seo<sup>1\*</sup>, Yanghee Kim<sup>2</sup>, Ji Yeong Lee<sup>2</sup>, Sugyeong Hong<sup>3</sup>, Sun Hee Kim<sup>3</sup>, Jung-Keun Lee<sup>4\*</sup>

<sup>1</sup>Division of Advanced Materials, Korea Research Institute of Chemical Technology, Daejeon, Korea

<sup>2</sup>Advanced Analysis Center, Korea Institute of Science and Technology, Seoul, Korea

<sup>3</sup>Western Seoul Center, Korea Basic Science Institute, Seoul, Korea

<sup>4</sup>Physics Department, Division of Liberal Arts & Sciences, Hanil University & PTS, Wanju, Korea

Email: \*jwseo@kRICT.re.kr, \*jklee@jbnu.ac.kr

**How to cite this paper:** Jeon, N.J., Seo, J., Kim, Y., Lee, J.Y., Hong, S., Kim, S.H. and Lee, J.-K. (2022) Focused-Ion-Beam Induced Paramagnetic Defects in FAMn:PbI<sub>3</sub> Perovskite Films. *Advances in Chemical Engineering and Science*, 12, 87-95.

<https://doi.org/10.4236/aces.2022.122007>

**Received:** January 4, 2022

**Accepted:** March 21, 2022

**Published:** March 24, 2022

Copyright © 2022 by author(s) and Scientific Research Publishing Inc.

This work is licensed under the Creative Commons Attribution International License (CC BY 4.0).

<http://creativecommons.org/licenses/by/4.0/>



Open Access

## Abstract

FAMn:PbI<sub>3</sub> perovskite films were synthesized and probed mainly through electron spin resonance (ESR) spectroscopy. FAMn:PbI<sub>3</sub> with low (~1%) Mn concentration showed a hyperfine sextet line originated from Mn<sup>2+</sup> ions. FAMn:PbI<sub>3</sub> with high (10%) Mn concentration showed broad resonance (~500 G peak-to-peak linewidth). However, after bombardment of FAMn:PbI<sub>3</sub> with high Mn concentration by focused ion beams (FIB), a sharp ESR peak appeared. The peak-to-peak linewidth ( $\Delta H_{pp}$ ) was ~8 G regardless of the temperature. The FIB-induced defect showed Curie behavior at low temperatures (5 K - 50 K), which indicates the presence of localized electrons at the defect sites at low temperatures. The g-value increased from  $g = 2.0002$  to 2.0016 as the temperature increased from 5 K to 50 K. Together with the ongoing search for electron spin echo (ESE), this could potentially provide a platform for realizing magnetic bits, information storage, and increased manipulation speed.

## Keywords

Perovskite Manganites, FIB, Paramagnetic Spins

## 1. Introduction

While methylammonium lead iodide (MAPbI<sub>3</sub>) has led to the development of prototype technology, perovskite solar cells (PSCs), formamidinium lead iodide (FAPbI<sub>3</sub>) has also attracted much attention [1] [2] [3]. To date, PSCs with photo conversion efficiencies (PCEs) of >25% mainly use FAPbI<sub>3</sub>-dominated perovs-

kite as a light absorber due to their superior opto-electrical properties, narrower band gap, longer charge-diffusion length, and better photostability and thermostability [4] [5].

Perovskite manganites may provide a useful material platform for new magnetic materials [6]. MAMn:PbI<sub>3</sub> has been studied by Náfrádi *et al.*, who found that photo-excited electrons melt the local magnetic order in the ferromagnetic photovoltaic MAMn:PbI<sub>3</sub> [7]. Technologically relevant materials may emerge when the magnetic interactions of spins are present and competing to determine the ground state. This may provide potential for realizing magnetic bits, information storage, and increased manipulation speed [7] [8] [9].

Ion beam irradiation is also known to induce structural changes such as phase transitions and amorphization [10] [11] [12]. The focused ion beam (FIB) method has recently been used to tune the optical properties of lead halide perovskites, thus opening an interesting avenue for applications in optoelectronic devices [11].

In this work, we report that isolated and localized paramagnetic spins can be formed by employing FIB of perovskite manganites. We have found that isolated and localized paramagnetic spin sites were formed by the application of FIB onto FAMn:PbI<sub>3</sub> perovskite films. This may potentially provide a useful material platform for realizing magnetic bits, information storage, and increased manipulation speed.

## 2. Experimental

The fabrication of the FAPbI<sub>3</sub> and FAMn:PbI<sub>3</sub> thin films with thickness of about 400 nm has been carried out through two-step sequential deposition and solvent engineering representative of wet processes that can yield perovskite films for high-performance PSCs. In the sequential deposition process, a thin layer of PbI<sub>2</sub> is deposited on the substrate; formamidinium iodide (FAI) is then applied to the predeposited PbI<sub>2</sub> to enable conversion to the perovskite phase. This process involves crystal nucleation and growth of the perovskite phase because of solution-phase or solid state reaction between PbI<sub>2</sub> and an organic iodide such as FAI. Details of synthesizing FAPbI<sub>3</sub> films were described in previous publications [2] [10]. For the mixed halide perovskite FAMn:PbI<sub>3</sub> films, details were referred from a reference [7].

To create defects, a focused ion beam (FIB, Hitachi-NX5000) was used. The specimens were irradiated using a Ga ion beam. Ion beam irradiation conditions were: acceleration voltage 30 keV, beam current 65 nA (6 s at ~100 K). A vacuum of about  $1 \times 10^{-7}$  mbar was maintained inside the column Ga can be focused to a fine probe size (500  $\mu\text{m} \times 500 \mu\text{m}$ ).

ESR measurements were performed using X-band (9.64 GHz) Bruker EMXplus apparatus. For the ESR measurements, polyethylene terephthalate (PET)/perovskite layers were prepared. Room temperature and low-temperature (5 K - 50 K) measurements were carried out at low microwave powers, at which magnetic re-

sonance signals are in a non-saturated regime. Modulation frequency was 100 kHz. ESR intensities of the signals were calculated by double integration of the first derivative spectra.

### 3. Results and Discussion

**Figure 1** shows scanning electron microscopy (SEM) images of FAMn:PbI<sub>3</sub> perovskite films with high (10 %) Mn concentration before FIB (**Figure 1(a)**) and after FIB (**Figure 1(b)**). While the film before FIB shows a compact and pin-hole-free morphology; the film after FIB exhibits a smooth surface with some pin-holes. Any chemical or structural change in the surface may be responsible for the smooth surface.

In **Figure 2**, the absorption spectrum of the FAMn:PbI<sub>3</sub> film with high (10%)

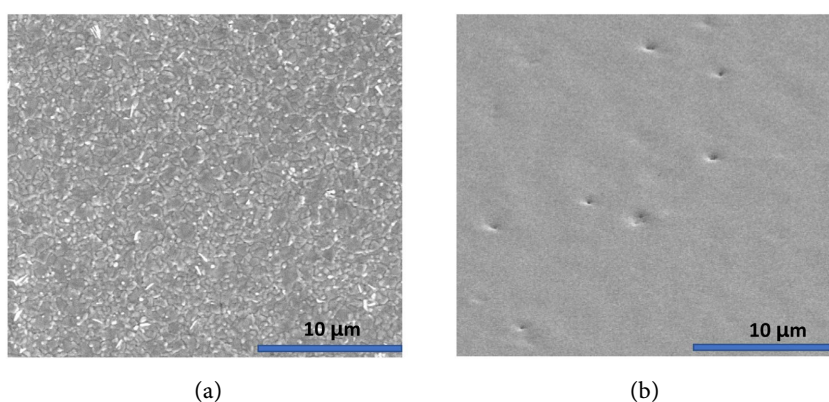


**Figure 1.** Scanning Electron Microscopy (SEM) images of room temperature perovskite films: FAMn:PbI<sub>3</sub> film before FIB treatment (a), and after FIB (b). Scale bar, 10  $\mu\text{m}$ .

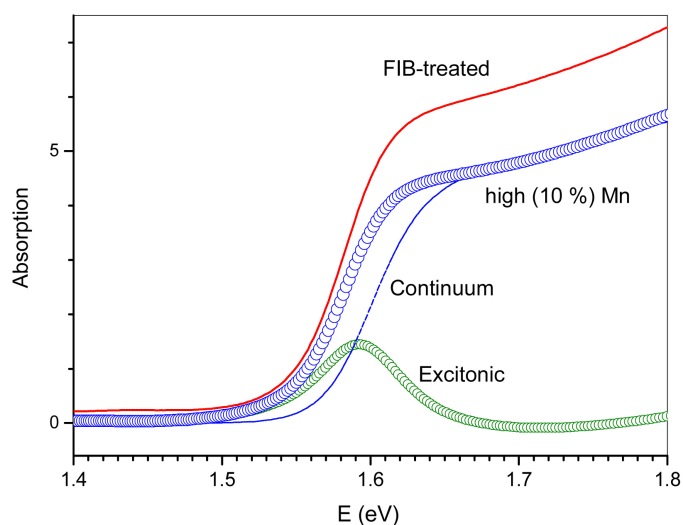


**Figure 2.** The absorption spectrum (blue open circle) of the FAMn:PbI<sub>3</sub> film with high (10%) Mn concentration (denoted as “high Mn”) near the bandgap was fit by Elliott’s model. The contribution from excitonic (green open circle line) and continuum band (blue dash line) transitions are also plotted. The absorption spectra of FIB-treated films (denoted as “FIB-treated”) are compared with the “high Mn”.

model. The absorption spectrum in direct semiconductors near the bandgap can be described using the Elliott formula, where the contributions of discrete exciton transitions are added to the continuum transitions [13]-[18].

Elliott's formula is given by:

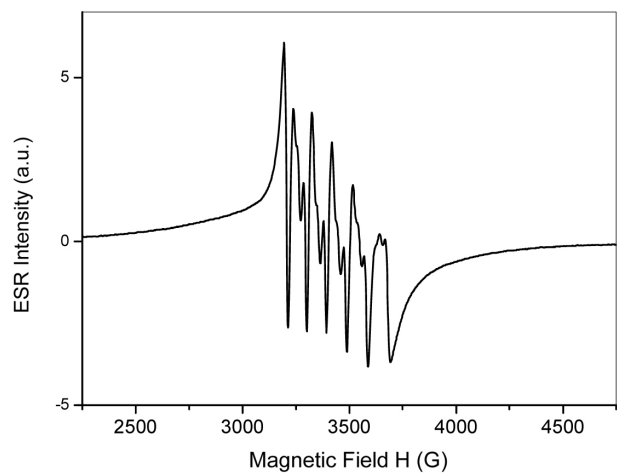
$$A(\omega) = A_0 \cdot \theta(\hbar\omega - E_g) \cdot \left( \frac{\pi e^{\pi x}}{\sinh(\pi x)} \right) + A_0 \cdot R_{ex} \sum_{n_{ex}=1}^{\infty} \frac{4\pi}{n_{ex}^3} \cdot \delta\left(\hbar\omega - E_g + \frac{R_{ex}}{n_{ex}^2}\right) \quad (1)$$

where  $A_0$  is a constant related to the transition matrix element;  $\omega$  is the frequency of light,  $\theta$  is the step function;  $E_g$  is the bandgap;  $x$  is defined as  $R_{ex}^{1/2} / (\hbar\omega - E_g)^{1/2}$ , where  $R_{ex}$  is the exciton binding energy;  $n_{ex}$  is the principal quantum number, and  $\Delta$  denotes a delta function. To account for inhomogeneous broadening, the continuum and excitonic part of Equation (1) are convolved with Gaussian functions. From the best fitting of the model, we extracted that the exciton resonance ( $E_0$ ) is centered at 1.589 eV. The bandgap ( $E_g$ ) of continuum transitions was found at 1.60 eV, which yields an exciton binding energy ( $R_{ex} = E_g - E_0$ ) of 11 meV. After FIB, we noted only an increase in absorption intensity after FIB.

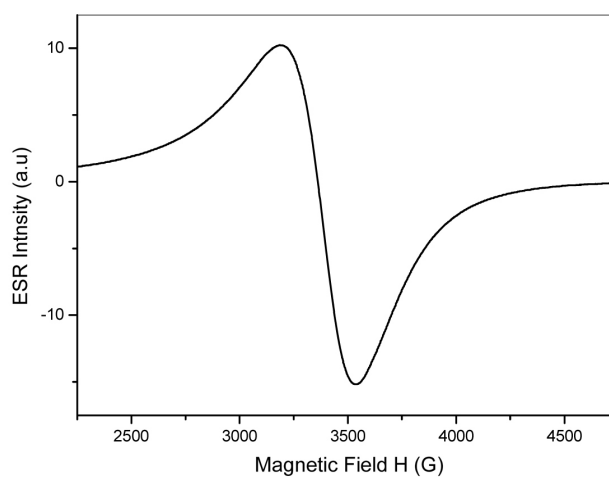
Pristine FAPbI<sub>3</sub> films showed no ESR spectrum. **Figure 3(a)** shows the ESR spectrum of FAMn:PbI<sub>3</sub> with low (~1%) Mn concentration (1 mW of microwave power). A manganese ion will result in an EPR feature with six hyperfine lines. FAMn:PbI<sub>3</sub> with low (~1%) Mn concentration showed a hyperfine sextet line originated from Mn<sup>2+</sup> ions. At low Mn concentrations, Náfrádi *et al.* also reported previously well-resolved hyperfine lines for MAMn:PbI<sub>3</sub> perovskite. [7].

Mn substitution with a high Mn concentration modified the magnetic properties of the system. **Figure 3(b)** shows the ESR spectra of FAMn:PbI<sub>3</sub> with high (10%) Mn concentration measured at 0.005 mW of microwave power at 10 K. We see a broad ESR line shape with a peak-to-peak linewidth ( $\Delta H_{pp}$ ) of about 500 G. Náfrádi *et al.* previously reported a broad paramagnetic signal (linewidth ~ about 500 G) from perovskite MAMn:PbI<sub>3</sub> [7]; they further also showed steeply increased linewidth at low temperatures (below 25 K), typical of ferromagnetic states. And they reported optically switched magnetism in perovskite MAMn:PbI<sub>3</sub>, where they observed that photo-excited electrons rapidly melt the local magnetic order [7].

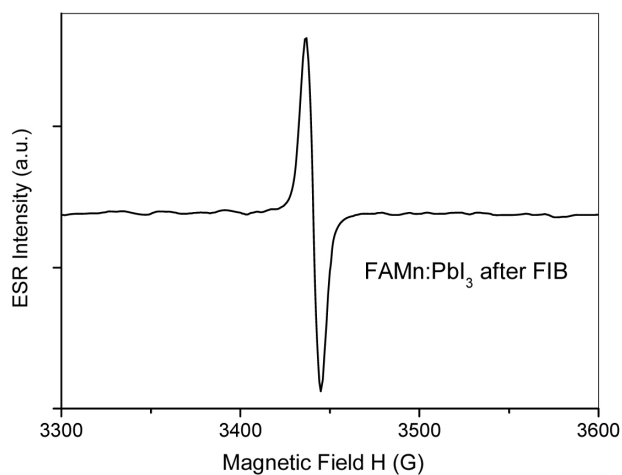
In **Figure 3(c)**, we have shown an ESR spectrum of FIB-treated perovskite FAMn:PbI<sub>3</sub> with high (10%) Mn concentration. The measurements were taken after FIB treatment on the FAMn:PbI<sub>3</sub> film to identify the formation of paramagnetic defects generated by a FIB-induced process. Surprisingly, a well-defined sharp ESR signal was generated after FIB-treatment of FAMn:PbI<sub>3</sub> as shown in **Figure 3(c)**. Specifically, the signal showed a  $g$ -value of 2.0034 and a peak-to-peak line width ( $\Delta H_{pp}$ ) of about 8 gauss. We obtained the sharp FIB-induced new peak only from the FAMn:PbI<sub>3</sub> with high (~10%) Mn concentration; but not from the FIB-treated FAMn:PbI<sub>3</sub> with dilute Mn concentration, nor from the FIB-treated FAMn:PbI<sub>3</sub> film with much higher Mn concentration. We note that



(a)



(b)



(c)

**Figure 3.** The ESR spectra of (a) FAMn:PbI<sub>3</sub> with low (~1%) Mn concentration (1 mW of microwave power), (b) FAMn:PbI<sub>3</sub> with high (10%) Mn concentration before FIB-treatment (0.005 mW of microwave power), and (c) FAMn:PbI<sub>3</sub> with high (10%) Mn concentration after FIB treatment.

the center of the broad resonance of FAMn:PbI<sub>3</sub> before FIB treatment is the same as that of the sharp FIB-induced new peak; *i.e.*, they have the same  $g$ -value ( $g = 2.0034$ ).

To determine the low-temperature properties of the defect center, ESR measurements were taken between 5 K and 50 K. **Figure 4(a)** shows the temperature-dependent variation at low temperatures (5 - 50 K) of the new ESR signal. It can be seen that the ESR intensity decreases with increasing temperature. The lineshape of the signal ( $g = 2.003$ ) is well fitted with a Lorentzian derivative lineshape, which implies that the isolated defect centers have relatively long spin-spin relaxation times [19]. The process of determining electron spin echo (ESE) with  $T_1$ ,  $T_2$  measurements is currently under investigation. This may potentially provide a platform for realizing magnetic bits, information storage, and increased manipulation speed.

In **Figure 4(b)**, the ESR intensity of the signals was calculated using a double integration of the first derivative spectra. The doubly integrated ESR intensity (which is proportional to spin density) varied linearly with the reciprocal temperature (as governed by Curie's law). This Curie behavior suggests that the

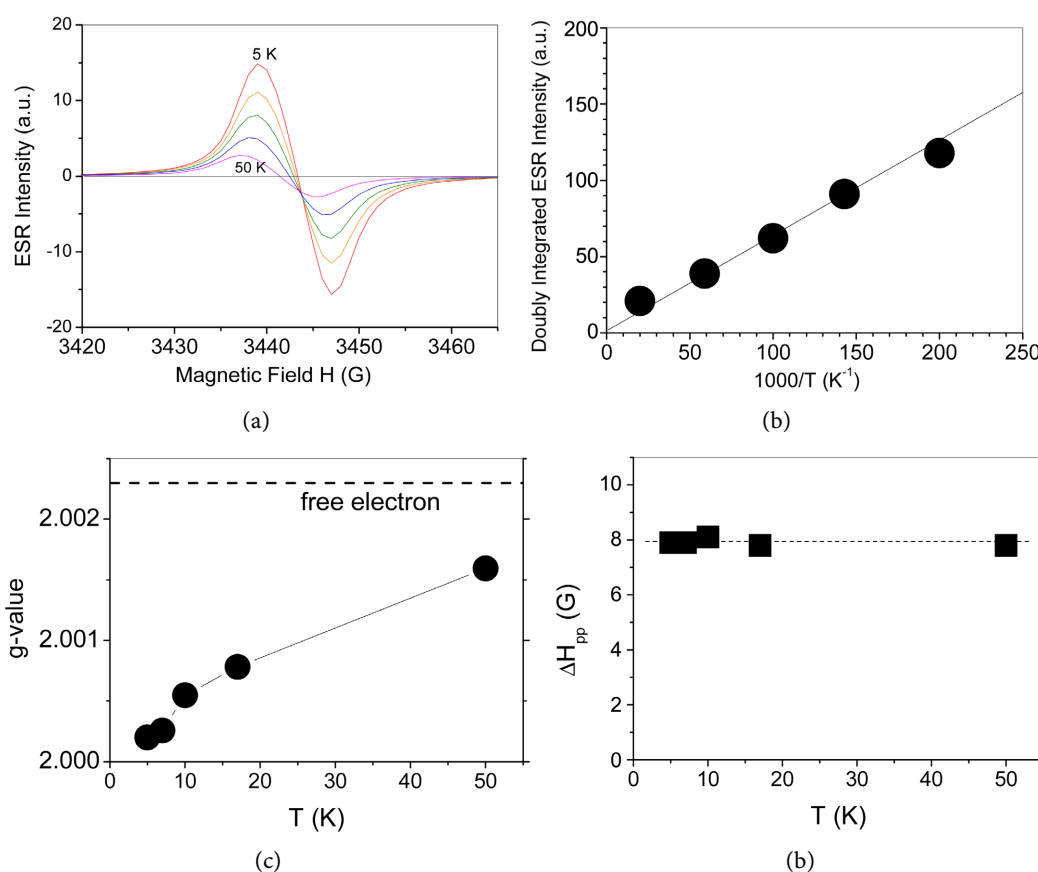


**Figure 4.** (a) Temperature-dependence of the ESR spectra of the new center (at 5, 7, 10, 17, 50 K). (b) Temperature-dependence of the doubly integrated ESR intensity. (c) The variation of the  $g$ -factor in the temperature range. (d) Temperature-independence of the ESR linewidth (The size of the data points in **Figure 4** correlate to the assumed error bar).

electronic wavefunction of the new defect is well localized at low temperatures. The number of isolated paramagnetic electrons does not vary over this temperature range [20]. A spin concentration of an order of  $\sim 10^{18} \text{ cm}^{-3}$  was obtained. It may also be noted that the number of holes on the surface in SEM (**Figure 1(b)**) was also roughly consistent with the order of  $\sim 10^{18} \text{ cm}^{-3}$ .

From the temperature-dependence of the ESR spectra, we can extract the temperature dependence of the  $g$ -factor (see **Figure 4(c)**) and the linewidth (see **Figure 4(d)**). As was shown in **Figure 3(b)**, the center of the wide resonance of FAMn:PbI<sub>3</sub> is the same as the center of the sharp FIB-induced new peak. Both may have the same origin. The only difference is that, in broad resonance, long distance spin correlation occurs, while isolated paramagnetic electronic spin contributes to the new FIB-induced sharp peak.

We note that the  $g$ -value increases with increasing temperature in this temperature range (5 - 50 K). The  $g$  value respectively increased from  $g = 2.0002$  to  $2.0016$  as the temperature increased from 5 K to 50 K. The  $g$ -factor change in the signal with respect to temperature may arise from additional spin correlations. **Figure 4(d)** shows the independence of the linewidth on the change in temperature at low temperatures (5 - 50 K). The linewidth ( $\Delta H_{pp} = 8 \text{ G}$ ) did not change with temperature.

#### 4. Conclusions

In conclusion, FAPbI<sub>3</sub> and FAMn:PbI<sub>3</sub> perovskite films were synthesized and treated by focused ion beam (FIB). The specimens were examined through SEM, optical absorption, and ESR spectroscopy.

While the film before FIB showed a compact and pinhole-free morphology, the films after FIB exhibited a smooth surface with some pin-holes.

The absorption spectrum was described using the Elliott formula. We extracted that the exciton resonance ( $E_0$ ) is centered at 1.589 eV. The bandgap ( $E_g$ ) of continuum transitions was found at 1.60 eV, yielding an exciton binding energy ( $R_{ex} = E_g - E_0$ ) of 11 meV. There were no considerable differences except for the absorption intensity between FAMn:PbI<sub>3</sub> and FIB-treated FAMn:PbI<sub>3</sub> perovskite films. Pristine FAPbI<sub>3</sub> showed no ESR signal. The ESR spectra of FAMn:PbI<sub>3</sub> with low ( $\sim 1\%$ ) Mn concentration showed an EPR feature with six hyperfine lines. FAMn:PbI<sub>3</sub> with high (10%) Mn concentration showed a broad ESR line shape with a peak-to-peak linewidth ( $\Delta H_{pp}$ ) of about 500 G.

Surprisingly, a sharp ESR peak appeared after bombardment by focused ion beams. The defect showed Curie behavior at low temperatures (5 to 50 K), which is indicative of localized electrons at the defect sites at low temperatures. The  $g$  value respectively increased from  $g = 2.0002$  to  $2.0016$  as the temperature increased from 5 K to 50 K; the linewidth ( $\Delta H_{pp}$ ) was  $\sim 8 \text{ G}$  regardless of the temperature variation. This may potentially lead to a platform for realizing perovskite manganese-based magnetic bits, information storage, and increased manipulation speed.

## Acknowledgements

This research was supported by a grant from the Korea Research Institute of Chemical Technology (KRICT) (SS2122-20). This research was also partly supported by the Basic Science Research Program through the National Research Foundation of Korea (NRF) funded by the Ministry of Education (2017R1D1A1B03028062). This research was also supported by the National Research Council of Science & Technology (NST) grant by the Korea government (MSIT) (No. CAP18054-200).

## Conflicts of Interest

The authors declare no conflicts of interest regarding the publication of this paper.

## References

- [1] Jeon, N.J., Noh, J.H., Yang, W.S., Kim, Y.C., Ryu, S., Seo, J. and Seok, S.I. (2015) Compositional Engineering of Perovskite Materials for High-Performance Solar Cells. *Nature*, **517**, 476-480. <https://doi.org/10.1038/nature14133>
- [2] Yang, W.S., Noh, J.H., Nam, J.J., Kim, Y.C., Ryu, S., Seo, J. and Seok, S.I. (2015) High-Performance Photovoltaic Perovskite Layers Fabricated through Intramolecular Exchange. *Science*, **348**, 1234-1237. <https://doi.org/10.1126/science.aaa9272>
- [3] Han, Q., Bae, S.-H., Sun, P., Hsieh, Y.-T., Yang, Y., Rim, Y.S., Zhao, H., Chen, Q., Shi, W., Li, G. and Yang, Y. (2016) Single Crystal Formamidinium Lead Iodide (FAPbI<sub>3</sub>): Insight into the Structural, Optical, and Electrical Properties. *Advanced Materials*, **28**, 2253-2258. <https://doi.org/10.1002/adma.201505002>
- [4] Chen, Z., Zhang, H., Yao, F., Tao, C., Fang, G. and Li, G. (2020) Room Temperature Formation of Semiconductor Grade  $\alpha$ -FAPbI<sub>3</sub> Films for Efficient Perovskite Solar Cells. *Cell Reports Physical Science*, **1**, Article ID: 100205. <https://doi.org/10.1016/j.xcrp.2020.100205>
- [5] Tan, S., Yavuz, I., Weber, M.H., Huang, T., Chen, C.-H., Wang, R., Wang, H.-C., Ko, J.H., Nuryyeva, S., Xue, J., Zhao, Y., Wei, K.-H., Lee, J.-W. and Yang, Y. (2020) Shallow Iodine Defects Accelerate the Degradation of  $\alpha$ -Phase Formamidinium Perovskite. *Joule*, **4**, 2426-2442. <https://doi.org/10.1016/j.joule.2020.08.016>
- [6] Xia, W., Pei, Z., Leng, K. and Zhu, X. (2020) Research Progress in Rare Earth-Doped Perovskite Manganite Oxide Nanostructures. *Nanoscale Research Letters*, **15**, Article No. 9. <https://doi.org/10.1186/s11671-019-3243-0>
- [7] Náfrádi, B., Szirmai, P., Spina, M., Lee, H., Yazzyev, O.V., Arakcheeva, A., Chernyshov, D., Gibert, M., Forró, L. and Horváth, E. (2016) Optically Switched Magnetism in Photovoltaic Perovskite CH<sub>3</sub>NH<sub>3</sub>(Mn:Pb)I<sub>3</sub>. *Nature Communications*, **7**, Article No. 13406. <https://doi.org/10.1038/ncomms13406>
- [8] Achermann, M., Hollingsworth, J.A. and Klimov, V.I. (2003) Multiexcitons Confined within a Subexcitonic Volume: Spectroscopic and Dynamical Signatures of Neutral and Charged Biexcitons in Ultrasmall Semiconductor Nanocrystals. *Physical Review B*, **68**, Article ID: 245302. <https://doi.org/10.1103/PhysRevB.68.245302>
- [9] Dey, A. and Yarlagadda, S. (2018) Temperature Dependence of Long Coherence Times of Oxide Charge Qubits. *Scientific Reports*, **8**, Article No. 3487. <https://doi.org/10.1038/s41598-018-21767-2>
- [10] Jeon, N.J., Yang, T.-Y., Park, H.H., Seo, J., Nam, D.Y., Jeong, D., Hong, S., Kim, S.H., Cho, J.M., Jang, J.J. and Lee, J.-K. (2019) Thermally Activated, Light-Induced

- Electron-Spin-Resonance Spin Density Reflected by Photocurrents in a Perovskite Solar Cell. *Applied Physics Letters*, **114**, Article ID: 013903. <https://doi.org/10.1063/1.5053830>
- [11] Qiao, L., Sun, X. and Long, R. (2019) Mixed Cs and FA Cations Slow Electron-Hole Recombination in FAPbI<sub>3</sub> Perovskites by Time-Domain *ab Initio* Study: Lattice Contraction versus Octahedral Tilting. *The Journal of Physical Chemistry Letters*, **10**, 672-678. <https://doi.org/10.1021/acs.jpcclett.8b03729>
- [12] Palei, M., Motapothula, M., Ray, A., Abdelhady, A.L., Lanzano, L., Prato, M., Panda, J.K., *et al.* (2020) Photoluminescence Enhancement and High Accuracy Patterning of Lead Halide Perovskite Single Crystals by MeV Ion Beam Irradiation. *Journal of Materials Chemistry C*, **8**, 9923-9930. <https://doi.org/10.1039/D0TC02326D>
- [13] D'Innocenzo, V., Grancini, G., Alcocer, M.J.P., Kandada, A.R.S., Stranks, S.D., Lee, M.M., Lanzani, G., Snaith, H.J. and Petrozza, A. (2014) Excitons versus Free Charges in Organo-Lead Tri-Halide Perovskites. *Nature Communications*, **5**, Article No. 3586. <https://doi.org/10.1038/ncomms4586>
- [14] Saba, M., Cadelano, M., Marongiu, D., Chen, F., Sarritzu, V., Sestu, N., Figus, C., Aresti, M., Piras, R., Lehmann, A.G., Cannas, C., Musinu, A., Quochi, F., Mura, A. and Bongiovanni, G. (2014) Correlated Electron-Hole Plasma in Organometal Perovskites. *Nature Communications*, **5**, Article No. 5049. <https://doi.org/10.1038/ncomms6049>
- [15] Sestu, N., Cadelano, M., Sarritzu, V., Chen, F., Marongiu, D., Piras, R., Mainas, M., Quochi, F., Saba, M., Mura, A. and Bongiovanni, G. (2015) Absorption F-Sum Rule for the Exciton Binding Energy in Methylammonium Lead Halide Perovskites. *The Journal of Physical Chemistry Letters*, **6**, 4566-4572. <https://doi.org/10.1021/acs.jpcclett.5b02099>
- [16] Yang, Y., Yang, M., Li, Z., Crisp, R., Zhu, K. and Beard, M.C. (2015) Comparison of Recombination Dynamics in CH<sub>3</sub>NH<sub>3</sub>PbBr<sub>3</sub> and CH<sub>3</sub>NH<sub>3</sub>PbBr<sub>3</sub> Perovskite Films: Influence of Exciton Binding Energy. *The Journal of Physical Chemistry Letters*, **6**, 4688-4692. <https://doi.org/10.1021/acs.jpcclett.5b02290>
- [17] Yang, Y., Yan, Y., Yang, M.J., Choi, S., Zhu, K., Luther, J.M. and Beard, M.C. (2015) Low Surface Recombination Velocity in Solution-Grown CH<sub>3</sub>NH<sub>3</sub>PbBr<sub>3</sub> Perovskite Single Crystal. *Nature Communications*, **6**, Article No. 7961. <https://doi.org/10.1038/ncomms8961>
- [18] Yang, Y., Yang, M., Zhu, K., Johnson, J.C., Berry, J.J., van de Lagemaat, J. and Beard, M.C. (2016) Large Polarization-Dependent Exciton Optical Stark Effect in Lead Iodide Perovskites. *Nature Communications*, **7**, Article No. 12613. <https://doi.org/10.1038/ncomms12613>
- [19] Jakes, P. and Erdem, E. (2011) Finite Size Effects in ZnO Nanoparticles: An Electron Paramagnetic Resonance (EPR) Analysis. *Physica Status Solidi—Rapid Research Letters*, **5**, 56-58. <https://doi.org/10.1002/pssr.201004450>
- [20] Cho, J.M., Seo, J.M., Lee, J.-K., Zhang, H. and Lamb, R. (2009) Electronic Properties of Oxygen Vacancies in Titania Nanotubes. *Physica B: Condensed Matter*, **404**, 127-130. <https://doi.org/10.1016/j.physb.2008.10.027>